INTERNATIONAL JOURNAL OF
ENERGY AND ENVIRONMENT

Volume 2, Issue 6, 2011 pp.1079-1100
Journal homepage: www.IJEE.IEEFoundation.org

Effect of turbulence in modeling the reduction of local drag forces in a computational automotive model

Sanwar A. Sunny

Department of Mechanical Engineering, School of Engineering, University of Kansas, Lawrence, KS 66045, USA.

Abstract
In this computational fluid dynamic (CFD) study on vehicle drag forces sheds light on the mathematical algorithms utilized to converge on pertinent data useful in the design and manufacture of automobiles. COSMOS Floworks™ was used to model the virtual vehicle motion involving various governing flow equations with main attention given to turbulent behavior in incompressible fluid flows. The paper highlighted Navier-Stokes considerations in the study and introduced Reynolds Decomposition methods to generate more refined models which in turn give accurate results, such as Reynolds-Averaged Navier–Stokes (RANS) Equations and Large Eddy Simulation (LES) Techniques, introduced using the Einstein Notation. Recent developments in Coherent vortex simulation methods were also briefly discussed. Example modeling and tests were conducted to show automotive design improvements that resulted in a 8.57% improvement in local drag forces (F_D) at the rear wheel wells, which effectively reduces the required Horsepower (hp) of the vehicle traveling at a certain speed (7.24 %). Different 3-D Automotive Design Models were examined in the current study, where real life design considerations and design benefits applications were briefly discussed. Furthermore, the paper highlights the need for utilization of both computational and real flow analysis on the car body and future performance relationship with the car's body weight, material and design.

Keywords: Automotive drag forces; Coefficient of drag; Reynolds-averaged Navier-Stokes equations; Large eddy simulation techniques; Reynolds decomposition.

1. Introduction

During automotive design, engineers usually model the exterior and perform varied tests to ensure smooth air flow over the car body. In recent years, the industry has effectively selected computer model simulation to replace archaic and massive wind turbines to conduct the aerodynamic tests to observe drag and lift behavior on all the external (and internal) vehicle components. However, to correctly converge on key design data that forecasts future on road performance, both real and virtual tests need to be conducted. In a conventional wind tunnel, the air velocity u is varied to observe the effects of the car's drag using the equation;

$$F_D = \frac{1}{2} C_D \rho_{air} A_{frontal} u^2 \tag{1}$$

From which the drag coefficient CD can be numerically computed using the equation:

$$C_D = \frac{F_D}{\frac{1}{2}\rho_{air} A_{frontal} u^2} \tag{2}$$

However in computer based wind tunnel tests, numerical algorithms replicated principles of Fluid Mechanics to solve and analyze systems dealing with compressible and incompressible flow of fluids. This branch is known as Computational Fluid Dynamics (CFD) and computers use preliminarily boundary conditions to simulate the interaction of fluids, perform calculations and obtain necessary results. This method is similar to Finite Element Method (FEA) Analysis. With CFD analysis, designers and engineers have the ability to change designs and conduct tests to compare aerodynamically sound designs without having to build different prototypes. Most software is cost effective in comparison to actual construction, fabrication and resulting analysis of prototypes. However, more advanced and precise CFD set ups are expensive.

To account for a precise value for the drag forces, certain key assumptions need to be addressed. The most important of which is the turbulence. Most wind tunnel flows are usually simulated with the Navier Stokes Equation [1] for precision and to take into analysis, the effect of the turbulence phenomenon. Turbulence is a time dependent chaotic behavior seen often in many fluid flows (including air flows) caused due to the inertia of the fluid as a whole to the culmination of time dependent acceleration; or flows where inertial behavior is insignificant and laminar. It is generally believed that the Navier–Stokes equations describe turbulence [2]. The numerical solution of the Navier–Stokes equations for turbulent flow is very complex, and due to the significantly different mixing-length scales involved in the turbulent flow, the solution of this model requires such an extremely fine mesh resolution in which the computational time becomes significantly unrealistic [3]. Solutions to turbulent flow using a laminar solving technique usually result in a time-unsteady figure, which does not converge appropriately.

However, certain models such as the Reynolds-Averaged Navier Stokes Equations (RANS) in addition to utilizing turbulence models can be used in to maintain a level of accuracy in Computational programs. In addition, Large Eddy Simulation (LES) can numerically solve for the correct data, however it has economic limitation as it is an expensive computation tool and is financially not viable for virtual model testing. LES techniques, although meticulous and expensive than the RANS model has the ability to yield better results, since in it, larger turbulent scales are appropriately resolved [4]. In this study, COSMOS Floworks, an add-in of SolidWorks will be utilized to conduct tests on design changes in a vehicle. Certain modeling restrictions will be addressed and different analysis methods will be briefly discussed. Finally, the design changes will be highlighted along with a reduction in overall drag forces and its effect on the fuel efficiency of the vehicle.

2. Mathematical analysis

Drag forces (F_D) of a car are depended on C_D, the coefficient of drag for the certain shape, ρ_{air}, the mass density of the fluid through which the body is traveling, $A_{frontal}$ or the vehicle's effective frontal area and most importantly u, the mean velocity of the car. $A_{frontal}$ is calculated both manually through photo pixelization and computationally through taking a section view and measuring the enclosed area in a 3-D CAD software such as Solidworks™ or 3-D StudioMAX™. The value of $A_{frontal}$ was computed at 0.0221 m^2. This is the effective area on which the majority of forces act. The forces vary according to another important parameter, the car's velocity, which in wind tunnels can be replicated as the air velocity travelling over a static car model.

2.1 Real wind tunnel modeling using Bernoulli's principle

The required expression for the velocity is given by using the algorithms of the Buckingham Pi Theorem, in which, the drag forces which are depend on the five above parameters can be quantified by two distinct mathematical expressions [5], which can be reduced using two dimensionless parameters culminating in the Reynolds number and finally yields the drag coefficient.

The function of five variables cane be effectively reduced by introducing a function of only two variables; where f_y is some function of two arguments.

$$f_x(F_D, u, A_{frontal}, \rho_{air}, v_0) = 0 \tag{3}$$

$$\mathrm{Re} = \frac{u\sqrt{A}}{v} \tag{4}$$

$$f_y\left(\frac{F_D}{\frac{1}{2}\rho_{air}A_{frontal}u^2}, \frac{u\sqrt{A}}{v}\right) = 0 \tag{5}$$

$$\frac{F_D}{\frac{1}{2}\rho_{air}A_{frontal}u^2} = f_z\left(\frac{u\sqrt{A}}{v}\right) \tag{6}$$

or

$$F_D = f_z\left(\frac{u\sqrt{A}}{v}\right).\left(\frac{1}{2}\rho_{air}A_{frontal}u^2\right) \tag{7}$$

$$\frac{1}{2}f_z(\mathrm{Re})\rho_{air}A_{frontal}u^2 \tag{8}$$

$$C_D = \left(\frac{2}{\rho_{air}A_{frontal}}\right)\left(\frac{F_D}{v_0^{\,2}}\right) \tag{9}$$

$$f_z(\mathrm{Re}) = C_D \tag{10}$$

$$F_D = \frac{1}{2}C_D\rho_{air}A_{frontal}u^2 \tag{11}$$

2.2 Work energy theorem

Certain elementary principles can be further used to derive Bernoulli's principle [6] which establishes a relationship between the velocity u and fluid height changes of a closed circuit manometer based wind tunnel [7].

$$W = \Delta E_k \tag{12}$$

Meaning that, the change in the kinetic energy E_k of the system is equal to the net work W done on the system; and the system itself consisting of a volume of incompressible fluid, between two distinct cross sectional areas given by A_1 and A_2 moving over the distances d_1 and d_2 respectively where $d_i=v_i\Delta t$.
The displaced fluid volumes are A_1d_1 and A_2d_2; implying that the displaced masses are ρA_1d_1 and ρA_2d_2, hence;

$$\rho A_1 d_1 = \rho A_1 v_1 \Delta t = \Delta m \tag{13}$$

and

$$\rho A_2 d_2 = \rho A_2 v_2 \Delta t = \Delta m \tag{14}$$

(with ρ being the fluid's mass density, Δt being the time interval through which the masses are displaced and the displaced mass denoted by Δm). The work done by pressure along the areas:

$$W_{\mathrm{p}} = F_{p,1}\, d_1 - F_{p,2}\, d_2 \tag{15}$$

$$p_1 A_1 d_1 - p_2 A_2 d_2 \tag{16}$$

$$\Delta m \frac{p_1}{\rho} - \Delta m \frac{p_2}{\rho} \tag{17}$$

the work done mostly by gravity (the gravitational potential energy in the volume $A_1 d_1$ is lost, and at the outflow in the volume $A_2 d_2$ is gained) [8] can be written as

$$\Delta E_g = \Delta m g z_2 - \Delta m g z_1 \tag{18}$$

$$W_{\mathrm{g}} = -\Delta E_g = \Delta m g z_1 - \Delta m g z_2 \tag{19}$$

the total work done in this time interval Δt being

$$W_t = W_g + W_p \tag{20}$$

$$\Delta E_k = \frac{1}{2}\Delta m u_2^2 - \frac{1}{2}\Delta m u_1^2 \tag{21}$$

$$\Delta m \frac{p_1}{\rho} - \Delta m \frac{p_2}{\rho} + \Delta m g z_1 - \Delta m g z_2 = \frac{1}{2}\Delta m u_2^2 - \frac{1}{2}\Delta m u_1^2 \tag{22}$$

$$\frac{1}{2}\Delta m u_1^2 + \Delta m g z_1 + \Delta m \frac{p_1}{\rho} = \frac{1}{2}\Delta m u_2^2 + \Delta m g z_2 + \Delta m \frac{p_2}{\rho} \tag{23}$$

$$\frac{1}{2}u_1^2 + g z_1 + \frac{p_1}{\rho} = \frac{1}{2}v_2^2 + g z_2 + \frac{p_2}{\rho} \tag{24}$$

$$\frac{1}{2}u^2 + g z + \frac{p}{\rho} = K \tag{25}$$

where K is a constant, where, multiplying by the fluid density (ρ) [9] throughout the equation

$$\frac{1}{2}\rho u^2 + \rho g z + p = K \tag{26}$$

or

$$q + \rho g h = p_0 + \rho g z = K \tag{27}$$

where q, h and p_0 gives the dynamic pressure head, hydraulic head and total pressure heads respectively,

$$q=\frac{1}{2}\rho u^2 \tag{28}$$

$$h=z+\frac{p}{\rho g} \tag{29}$$

$$p_0=p+q \tag{30}$$

Normalization of the constant in the equation gives another expression (*H* being the total energy head) which yields the expression for velocity *u.*

$$H=z+\frac{p}{\rho g}+\frac{u^2}{2g} \tag{31}$$

$$h+\frac{u^2}{2g} \tag{32}$$

$$H-h=\Delta h \tag{33}$$

$$u=\sqrt{2g\Delta h} \tag{34}$$

$$u=\sqrt{\frac{2SG\rho g\Delta h}{\rho_{air}}} \tag{35}$$

The height changes of manometer tube fluids in most wind tunnels signify changes in car speeds, at which the car experiences variable forces exerted by the moving air flow. Manual and computer data acquisition techniques are used to observe the changes, and force data results from these initial data being treated with expressions such as equation (2).

3. Turbulence in computation fluid flow modeling

With this analysis, real parameters are taken into consideration. In most computational study however, the wind velocity is not varied but, complex algorithms replicate real situations, and in doing so, can leave out important considerations such as turbulence.

There exists however, other advanced packages which conducts even more complex and time consuming iterations with a much larger and refined mesh and constrained boundary conditions. The Reynolds-averaged Navier–Stokes equations (or RANS equations) are time-averaged equations of motion for fluid flow. RANS expression results from the Reynolds decomposition, whereby an instantaneous quantity is decomposed into its time-averaged and fluctuating quantities.

3.1 Reynolds-averaged Navier–Stokes (RANS) equations

To study the theory of turbulence, Reynolds decomposition, a mathematical technique, is used to separate the average and fluctuating parts of a quantity. In computation fluid dynamics, the velocity *u,* which is given by;

$$u=\sqrt{\frac{2SG\rho g\Delta h}{\rho_{air}}} \tag{36}$$

in a real wind tunnel, can be treated with the decomposition technique as follows,

$$u(x,y,z,t) = \overline{u(x,y,z)} + u'(x,y,z,t) \tag{37}$$

where $\overline{u}$ denotes the time average of u (often called the steady component), and u' the fluctuating part, commonly known as perturbations. The perturbations are defined such that their time average equals zero.

This allows for the Navier-Stokes equations to be simplified by substituting the sum of the steady component and perturbations to the velocity profile and taking the mean value. The resulting equation contains a nonlinear term, the Reynolds stresses, which give rise to turbulence. The RANS equations can be used with approximations based on knowledge of the properties of flow turbulence to give approximate time-averaged solutions to the Navier–Stokes equations. For stationary and incompressible Newtonian fluids, the equations can be written in Einstein notation as:

$$\rho \frac{\partial \overline{u}_j \overline{u}_i}{\partial x_j} = \rho \overline{f}_i + \frac{\partial}{\partial x_j}\left[-\overline{p}\delta_{ij} + \mu\left(\frac{\partial \overline{u}_i}{\partial x_j} + \frac{\partial \overline{u}_j}{\partial x_i} \right) - \rho \overline{u_i' u_j'} \right] \tag{38}$$

where $\rho \frac{\partial \overline{u}_j \overline{u}_i}{\partial x_j}$ represents the change in mean momentum of fluid element owing to the unsteadiness in the mean flow and the convection by the mean flow.

This change is balanced by the mean body force $\rho \overline{f}$, the isotropic stress $\frac{\partial}{\partial x_j}\left[-\overline{p}\delta_{ij}\right]$ owing to the mean pressure field, the viscous stresses, $\mu\left[\frac{\partial \overline{u}_i}{\partial x_j} + \frac{\partial \overline{u}_j}{\partial x_i}\right]$ and apparent stress $\left(-\rho \overline{u_i' u_j'}\right)$ owing to the fluctuating velocity field, generally referred to as the Reynolds stress. This nonlinear Reynolds stress term requires additional modeling to close the RANS equation for solving, and has led to the creation of many different turbulence models. The time-average operator $\overline{\cdot}$ is a Reynolds operator.

The properties of Reynolds operators are useful in the derivation of the RANS equations. Using these properties, the Navier–Stokes equations of motion, expressed in tensor notation, are (for an incompressible Newtonian fluid);

$$\frac{\partial u_i}{\partial x_i} = 0 \tag{39}$$

Hence;

$$\frac{\partial u_i}{\partial t} + u_j \frac{\partial u_i}{\partial x_j} = f_i - \frac{1}{\rho}\frac{\partial p}{\partial x_i} + \nu \frac{\partial^2 u_i}{\partial x_j \partial x_j} \tag{40}$$

where f_i is a vector representing external forces. Each instantaneous quantity can be split into time-averaged and fluctuating components, and the resulting equation time-averaged, to yield;

$$\frac{\partial \overline{u_i}}{\partial x_i} = 0 \tag{41}$$

So;

$$\frac{\partial \overline{u_i}}{\partial t}+\overline{u_j}\frac{\partial \overline{u_i}}{\partial x_j}+\overline{u_j'\frac{\partial u_i'}{\partial x_j}}=\overline{f_i}-\frac{1}{\rho}\frac{\partial \overline{p}}{\partial x_i}+\nu\frac{\partial^2 \overline{u_i}}{\partial x_j \partial x_j} \tag{42}$$

Splitting each instantaneous quantity into its averaged and fluctuating components yields;

$$\frac{\partial\left(\overline{u_i}+u_i'\right)}{\partial x_i}=0 \tag{43}$$

or

$$\frac{\partial\left(\overline{u_i}+u_i'\right)}{\partial t}+\left(\overline{u_j}+u_j'\right)\frac{\partial\left(\overline{u_i}+u_i'\right)}{\partial x_j} \tag{44}$$

or

$$\left(\overline{f_i}+f_i'\right)-\frac{1}{\rho}\frac{\partial\left(\overline{p}+p'\right)}{\partial x_i}+\nu\frac{\partial^2\left(\overline{u_i}+u_i'\right)}{\partial x_j \partial x_j} \tag{45}$$

Time-averaging these equations yields,

$$\overline{\frac{\partial\left(\overline{u_i}+u_i'\right)}{\partial x_i}}=0 \tag{46}$$

$$\overline{\frac{\partial\left(\overline{u_i}+u_i'\right)}{\partial t}}+\overline{\left(\overline{u_j}+u_j'\right)\frac{\partial\left(\overline{u_i}+u_i'\right)}{\partial x_j}} \tag{47}$$

and

$$\overline{\left(\overline{f_i}+f_i'\right)}-\frac{1}{\rho}\overline{\frac{\partial\left(\overline{p}+p'\right)}{\partial x_i}}+\nu\overline{\frac{\partial^2\left(\overline{u_i}+u_i'\right)}{\partial x_j \partial x_j}}. \tag{48}$$

Simplifying nonlinear terms ($\overline{u_i u_i}$) yields ;

$$\overline{u_i u_i}=\overline{\left(\overline{u_i}+u_i'\right)\left(\overline{u_i}+u_i'\right)}=\overline{\overline{u_i}\,\overline{u_i}+\overline{u_i}u_i'+u_i'\overline{u_i}+u_i'u_i'}=\overline{u_i}\,\overline{u_i}+\overline{u_i'u_i'} \tag{49}$$

where the momentum equation can also be written as;

$$\frac{\partial \overline{u_i}}{\partial t}+\frac{\partial \overline{u_j}\,\overline{u_i}}{\partial x_j}=\overline{f_i}-\frac{1}{\rho}\frac{\partial \overline{p}}{\partial x_i}+\nu\frac{\partial^2 \overline{u_i}}{\partial x_j \partial x_j}-\frac{\partial \overline{u_i'u_j'}}{\partial x_j}. \tag{50}$$

and due to the conservation of mass equation, $\frac{\partial u_i}{\partial x_i}=\frac{\partial \overline{u_i}}{\partial x_i}+\frac{\partial u_i'}{\partial x_i}=0$ or further treatment yields;

$$\rho\frac{\partial\overline{u_i}}{\partial t}+\rho\frac{\partial\overline{u_j}\,\overline{u_i}}{\partial x_j}=\rho\overline{f_i}+\frac{\partial}{\partial x_j}\left[-\overline{p}\delta_{ij}+2\mu\overline{S_{ij}}-\rho\overline{u_i'u_j'}\right] \tag{51}$$

where, $\overline{S_{ij}}$ is the mean rate of strain tensor given by $\overline{S_{ij}}=\frac{1}{2}\left(\frac{\partial\overline{u_i}}{\partial x_j}+\frac{\partial\overline{u_j}}{\partial x_i}\right)$ where eliminating the time derivative yields;

$$\rho\frac{\partial\overline{u_j}\,\overline{u_i}}{\partial x_j}=\rho\overline{f_i}+\frac{\partial}{\partial x_j}\left[-\overline{p}\delta_{ij}+2\mu\overline{S_{ij}}-\rho\overline{u_i'u_j'}\right] \tag{52}$$

3.2 Large eddy simulation techniques

Another technique used for turbulence modeling is the Large Eddy Simulation (LES) Technique. LES is prevalent in a wide variety of engineering applications, including combustion, acoustics, and even simulations of the atmospheric boundary layer [10-12].

LES operates on the Navier-Stokes equations to reduce the range of length scales of the solution, reducing the computational cost. In mathematical Einstein notation, the Navier-Stokes equations for an incompressible fluid are:

$$\frac{\partial u_i}{\partial x_i}=0 \tag{53}$$

or

$$\frac{\partial u_i}{\partial t}+\frac{\partial u_iu_j}{\partial x_j}=-\frac{1}{\rho}\frac{\partial p}{\partial x_i}+\nu\frac{\partial^2u_i}{\partial x_j\partial x_j} \tag{54}$$

Taking out the momentum equation results in;

$$\frac{\partial\overline{u_i}}{\partial t}+\frac{\overline{\partial u_iu_j}}{\partial x_j}=-\overline{\frac{1}{\rho}\frac{\partial p}{\partial x_i}}+\nu\overline{\frac{\partial^2u_i}{\partial x_j\partial x_j}}. \tag{55}$$

then;

$$\frac{\partial\overline{u_i}}{\partial t}+\frac{\overline{\partial u_iu_j}}{\partial x_j}=-\frac{1}{\rho}\frac{\partial\overline{p}}{\partial x_i}+\nu\frac{\partial^2\overline{u_i}}{\partial x_j\partial x_j} \tag{56}$$

This equation models the changes in time of the filtered variables $\overline{u_i}$. Since the unfiltered variables u_i are not known, it is impossible to directly calculate $\frac{\overline{\partial u_iu_j}}{\partial x_j}$. However, since the quantity $\frac{\partial\overline{u_i}\,\overline{u_j}}{\partial x_j}$ is known. A substitution is made:

$$\frac{\partial\overline{u_i}}{\partial t}+\frac{\partial\overline{u_i}\,\overline{u_j}}{\partial x_j}=-\frac{1}{\rho}\frac{\partial\overline{p}}{\partial x_i}+\nu\frac{\partial^2\overline{u_i}}{\partial x_j\partial x_j}-\left(\frac{\overline{\partial u_iu_j}}{\partial x_j}-\frac{\partial\overline{u_i}\,\overline{u_j}}{\partial x_j}\right) \tag{57}$$

Suppose

$$\tau_{ij} = \overline{u_i u_j} - \overline{u_i}\,\overline{u_j} \,. \tag{58}$$

Hence, the resulting sets of equations are the LES equations;

$$\frac{\partial \overline{u_i}}{\partial t} + \overline{u_j}\frac{\partial \overline{u_i}}{\partial x_j} = -\frac{1}{\rho}\frac{\partial \overline{p}}{\partial x_i} + \nu\frac{\partial^2 \overline{u_i}}{\partial x_j \partial x_j} - \frac{\partial \tau_{ij}}{\partial x_j} \tag{59}$$

Other turbulence models include the direct numerical simulation, Detached Eddy simulation and the Coherent vortex simulation. However, they are used for extremely complex models and recent developments allow for preconditioners that deliver mesh-independent convergence rates for any given system [13].

4. Results and discussions

The first objective of this study was to evaluate the effect of turbulence in testing the behavior of drag forces in a computational study of an automobile. This was done by comparing data from real and computation fluid flows. Figure 1 shows the actual car, while Figure 2 shows its equivalent computational model. A previous experiment of a scaled (1:10) model in an actual wind tunnel (shown in Figure 3) was compared to computational studies (shown in Figures 4 and 5) to briefly look at the differences in real and computational results.

4.1 Drag forces effect in a wind tunnel

As described above, the expression uses the changes in tube heights (Δh) to denote corresponding air velocities (u). F_D is given from force balances in the wind chamber as shown in Table 1. Hence, we know from Eq (1) that, $C_D = F_D \Big/ \left(0.5\rho_{air} A_{frontal} u^2\right)$ and as the data from Table 1 show, at velocity u (mph), the drag forces F_D extended on the body with an effective frontal area $A_{Frontal}$ of 0.0221 m^2 with a standard mass density of air at 1.184 kg/m^3, the coefficient of drag C_D is given by equation 1 (at 68.14 mph) where C_D is found to be 0.40 as shown in Figure 6 [14]. This is quite less than the real drag coefficient value of 0.44 supplied by the manufactures (Volkswagen) [15]. This is due to the fact, that wheels and other external body parts, such as side mirrors, under-chassis, air dam etc, were excluded in the scaled epoxy model as shown in Figure 6.

Table 1. Wind tunnel test data on a scaled model

Total Height *H (cm)*	Height Change *Δh (m)*	Drag Force *F_D (N)*	Velocity *u (mph)*
8.00	0.01	0.80	29.79
9.70	0.03	2.00	45.26
10.50	0.04	2.49	50.94
11.30	0.05	3.20	56.05
12.00	0.06	3.65	60.16
13.50	0.07	4.80	68.14
14.10	0.08	5.34	71.09
15.20	0.09	6.23	76.19
16.50	0.10	7.16	81.80

Figure 1. Actual car without front and rear wheel wells and fenders

Note: The fenders are to be tested with design changes and resulting impacts on aerodynamics, mainly reduction of drag forces on the local area will be observed in this computational study.

Figure 2. Full scale car CAD model used to replicate air flow behaviour of an actual car
Note: See Figure 1 for a picture of the real car in question.

Figure 3. (1:10) scaled car model in the wind chamber of the closed circuit wind tunnel
Note: The body is made of clay-like material.

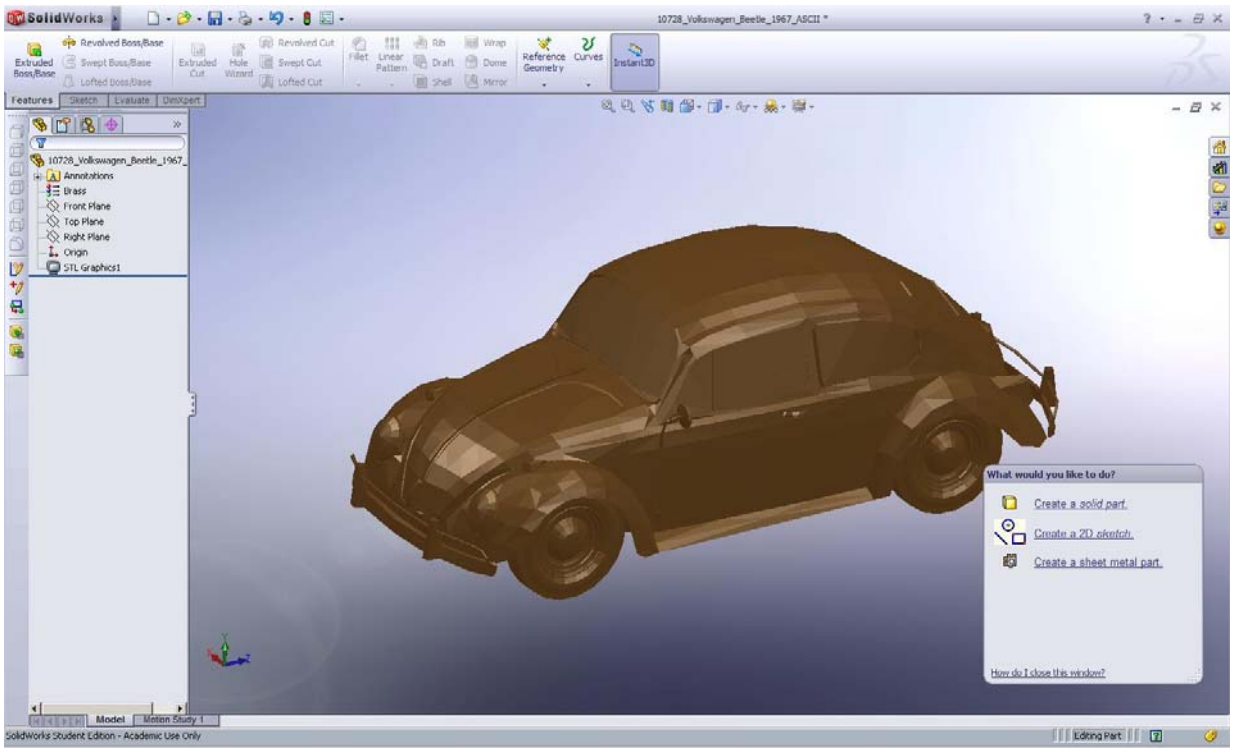

Figure 4. Full scale computational car model in virtual wind tunnel of COSMOS Floworks™
Note: The material chosen is clay to replicate previous conditions of the actual wind tunnel tests.

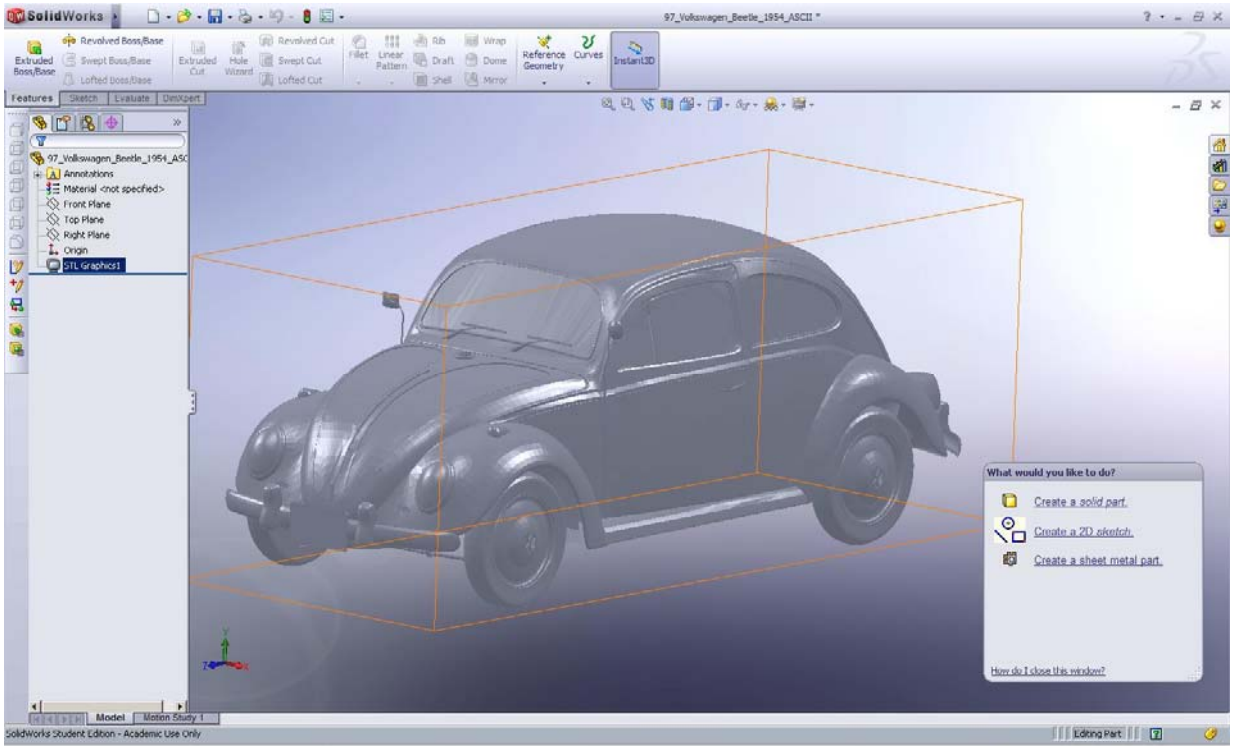

Figure 5. Full scale computational car model in virtual wind tunnel of COSMOS Floworks™
Note: The material used now is the conventional sheet metal used during the manufacture of the car.

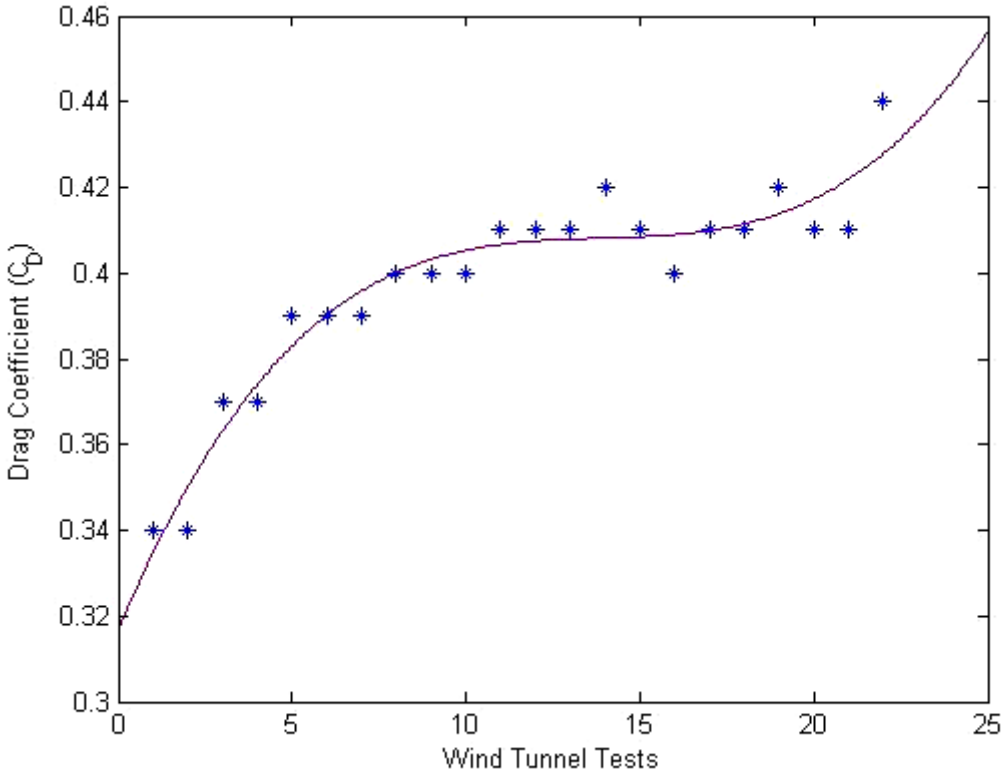

Figure 6. The mean value for the Drag Coefficients over tests ($C_D = 0.40$)

4.2 Computational or virtual wind tunnel testing

Again, using Equations (1) and (2), we can find the drag coefficient of the car which is in essence traveling at 55 f/s (or 16.76 m/s) and experiencing 353.61 lbf (1572.92 kg.m/s^2) of drag forces, with a frontal area $A_{frontal}$ of 22.10 m^2 (since the car is 10 times the model, area is 100 times the model) and ρ_{air} of 1.184 kg/m^3, as again, we know from equation 1 that given data from the CFD test yields a C_D of 0.428. This value is much closer to the literature data provided by manufacturers at 0.44 which is due to greater resemblance to the actual car than the scaled model. Hence, it can be said with a certain degree of accuracy that 0.012 differences in the coefficients are attributed to the turbulence during testing. These discrepancies can be reduced to an extent and even eliminated altogether by utilizing a more refined mesh and paying special attention to and the incorporation of the turbulence factor during complex computational iteration, as described above.

The second objective of the current study was to demonstrate the changes in design that lead to a reduced drag force being experienced by the automobile during motion at a certain speed. Design changes were made in a CAD software, to the rear wheel wells or fenders existing in the current vehicle. The model was then tested in the virtual wind tunnel of COSMOS Floworks to observe the changes in aerodynamics between the earlier and later designs.

Tables 2 and 3 show the data from the computational tests both before and after incorporating changes in designs of the rear wheel wells. The car without wheel skirts travelling at an average speed of 28 ft/sec experiences 3.5 lbf of force on it, while a car with the skirts travelling at the same speed experiences a force of around 3.2 lbf. Figures 7 and 8 shows the schematics for the fender skirts. That is an 8.57% reduction in the local drag force (F_D). Figure 9 shows the flow models. This design enhancement and the resulting improvement of aerodynamic follow will in turn change the required horsepower of the car, as shown in Table 4.

Table 2. Drag forces on fenders without wheel skirts

Goal Name	Unit	Value	Averaged Value	Minimum Value	Maximum Value
u_{min}	ft/s	0	0	0	0
u_{mean}	ft/s	28.06	28.07	28.05	28.15
u_{max}	ft/s	55	55	55	55
F_D	lbf	3.51	3.51	3.48	3.52
$F_{D,x}$	lbf	2.52	2.54	2.52	2.56
$F_{D,y}$	lbf	-1.22	-1.21	-1.28	-1.14
$F_{D,z}$	lbf	2.12	2.10	2.07	2.12

Table 3. Drag forces on fenders with wheel skirts

Goal Name	Unit	Value	Averaged Value	Minimum Value	Maximum Value
u_{min}	ft/s	0	0	0	0
u_{mean}	ft/s	28.06	28.07	28.05	28.15
u_{max}	ft/s	55	55	55	55
F_D	lbf	3.159	3.177	3.156	3.178
$F_{D,x}$	lbf	2.48	2.47	2.38	2.36
$F_{D,y}$	lbf	-1.19	-1.21	-1.23	-1.04
$F_{D,z}$	lbf	2.08	2.98	2.06	2.12

Table 4. Drag, Frictional and Supplied force reductions and their relationship with overall HP requirement

u	F_{RR}		f_{rr}	F_D		F_{sup}		Horsepower (hp_{sup})	
(mph)	Normal	Improved		Normal	Improved	Normal	Improved	Normal	Improved
30	28.44	25.95	0.0142	21.28	19.89	47.23	19.90	3.98	3.67
35	29.98	27.36	0.0144	28.97	27.07	56.32	27.09	5.50	5.08
40	31.52	28.76	0.0146	37.84	35.36	66.60	35.37	7.40	6.84
45	33.07	30.17	0.0149	47.89	44.75	78.06	44.77	9.71	8.99
50	34.61	31.58	0.0151	59.12	55.25	90.70	55.27	12.50	11.58
55	36.15	32.99	0.0153	71.53	66.85	104.52	66.87	15.79	14.64
60	37.70	34.39	0.0155	85.13	79.56	119.52	79.58	19.65	18.23
65	39.24	35.80	0.0158	99.91	93.37	135.71	93.39	24.12	22.39
70	40.78	37.21	0.0160	115.87	108.29	153.08	108.31	29.24	27.16
75	42.33	38.62	0.0162	133.01	124.31	171.63	124.33	35.07	32.59

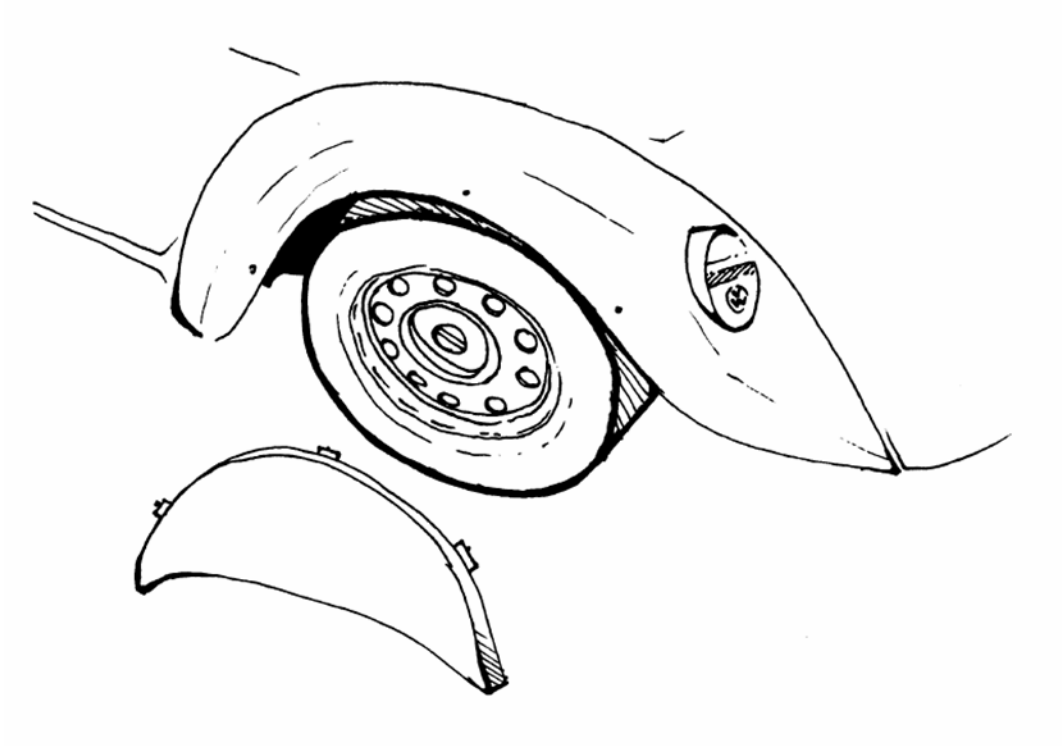

Figure 7. Metal skirts being applied to the wheel wells to deflect air flow away from the wheels
Note: This design enhancement can only be done to the rear wheels as such changes to the front wheels will impair their ability to turn.

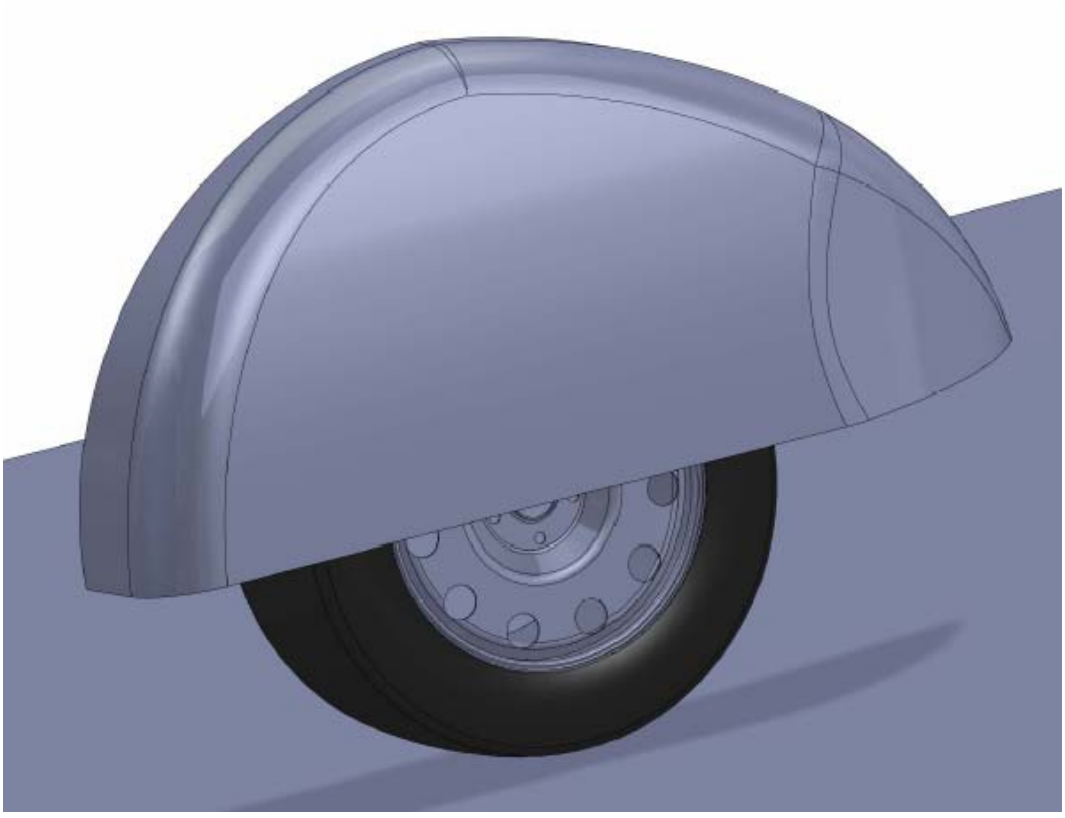

Figure 8. Computational local model of the enhanced design for the car's rear wheel wells in Solidworks™
Note: For reducing iteration time and complexity, the rest of the car was not used in testing.

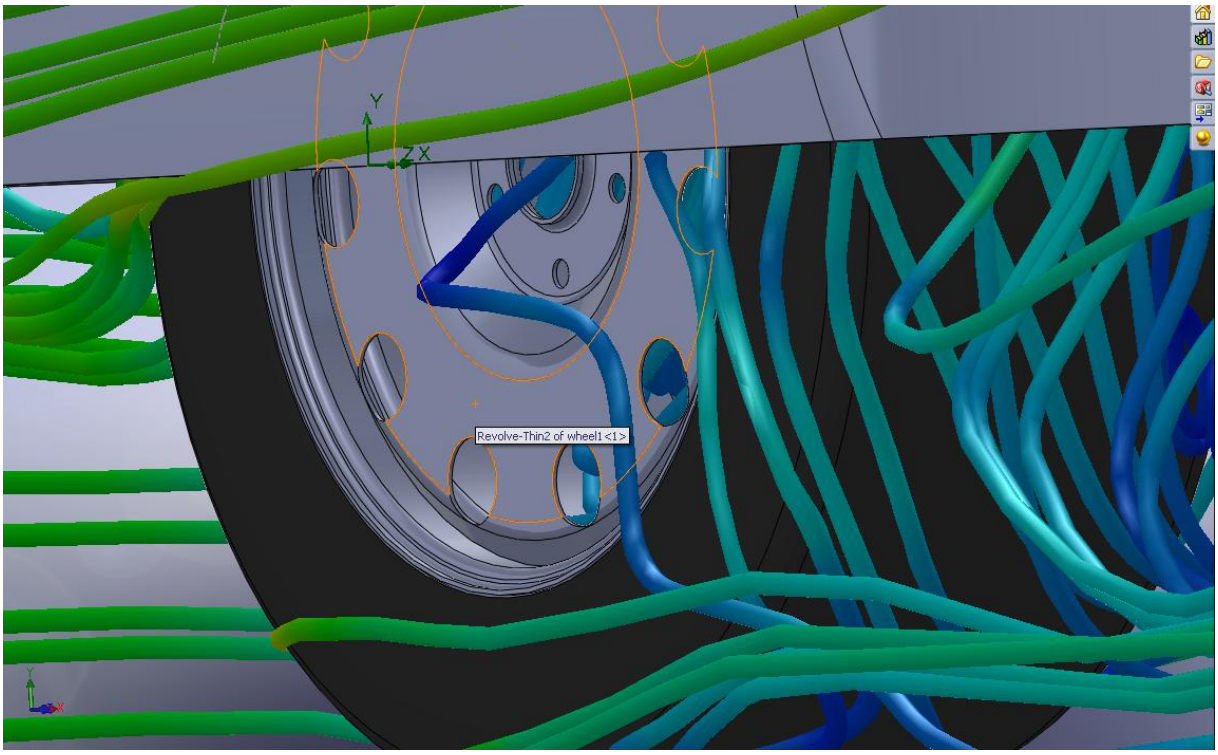

(a)

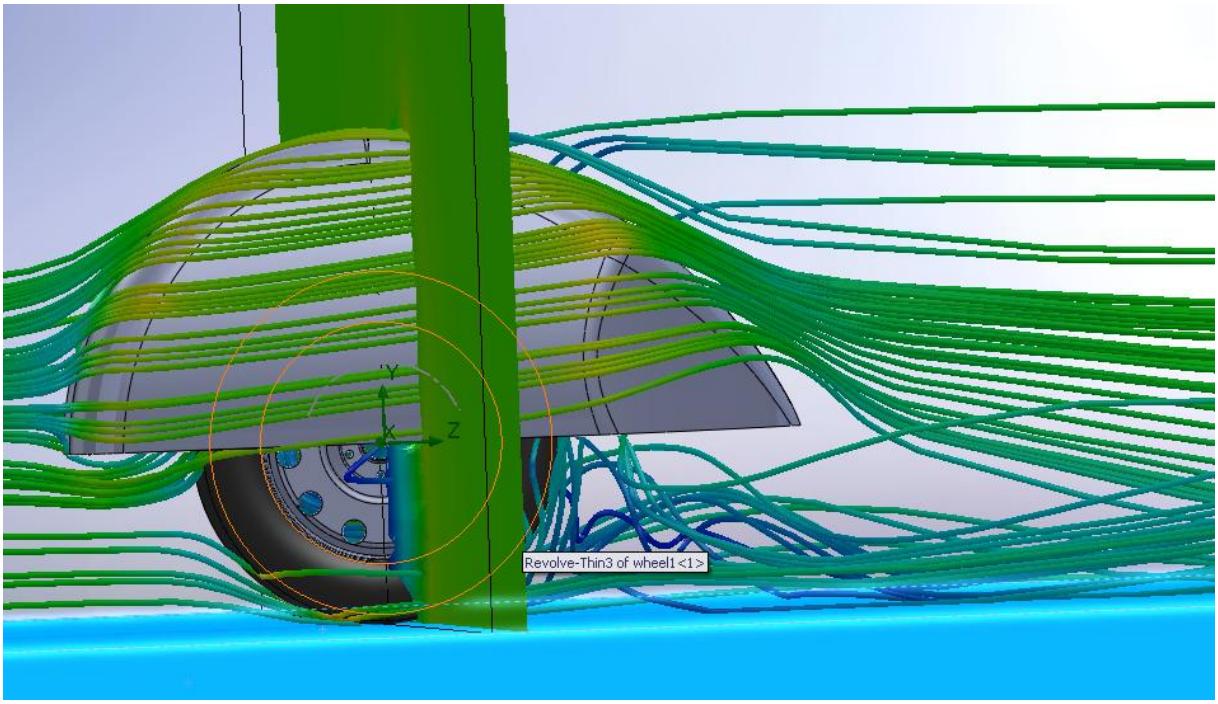

(b)

Figure 9. (Continued)

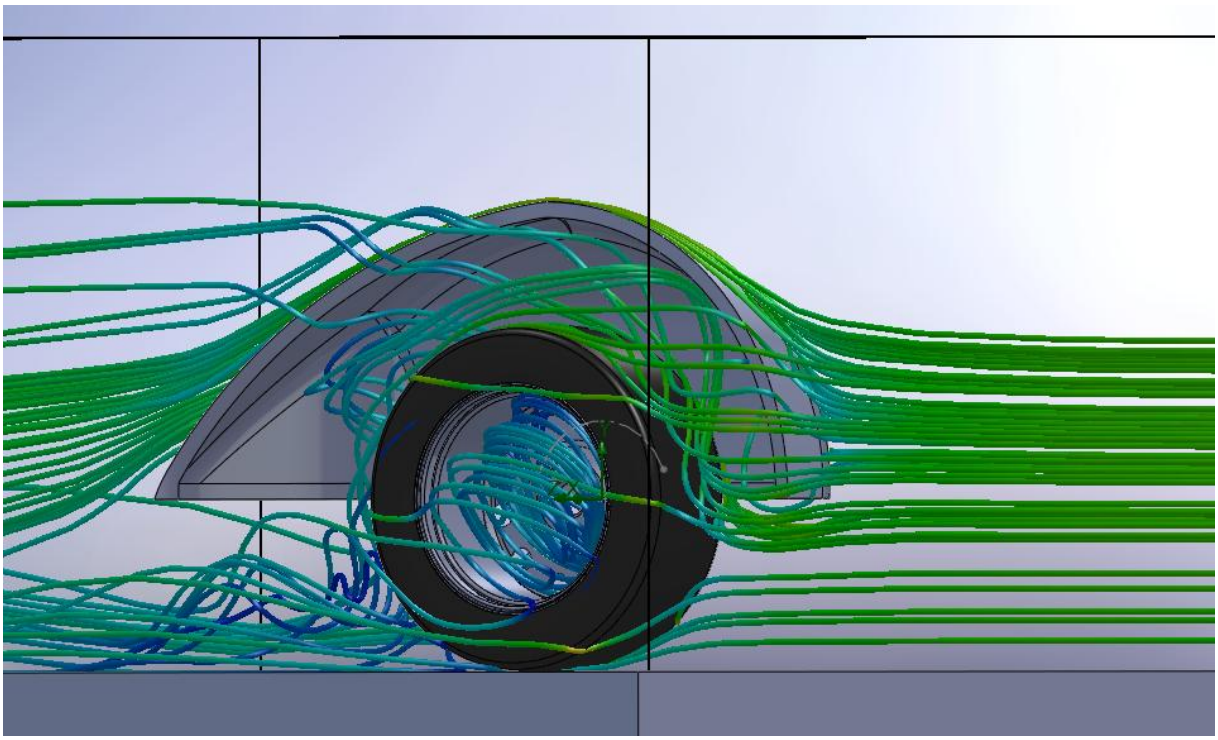

(c)

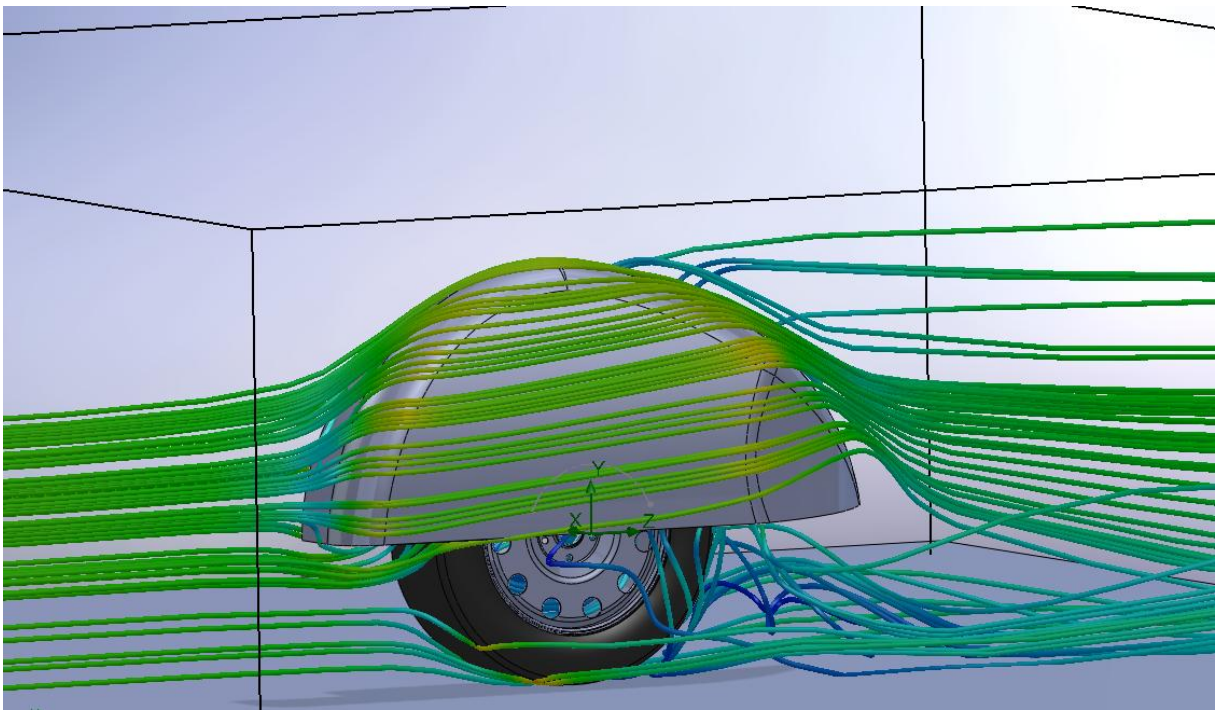

(d)

Figure 9. (Continued)

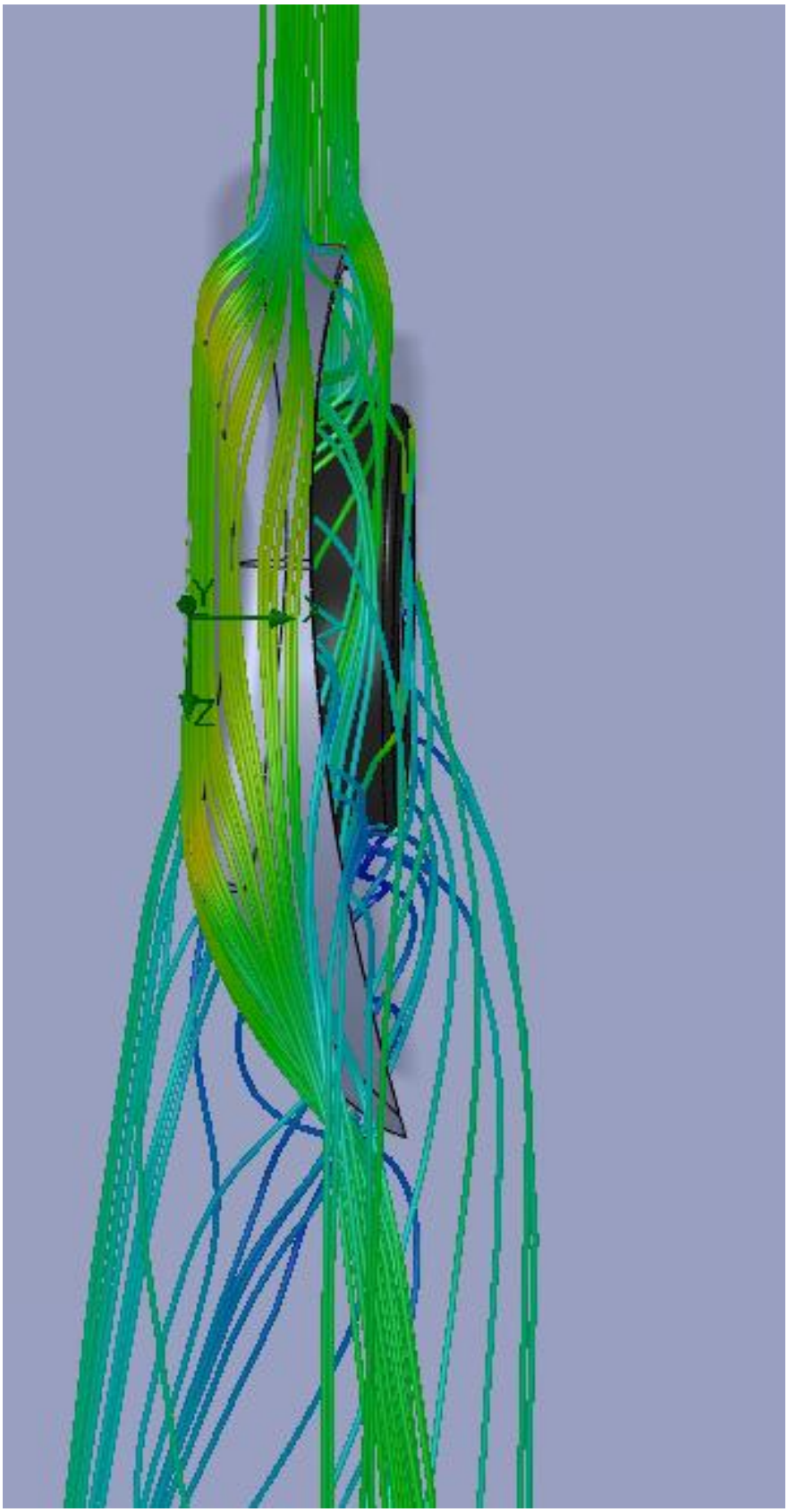

(e)

Figures 9. Detailed CFD tests shows the behavior of dynamic air

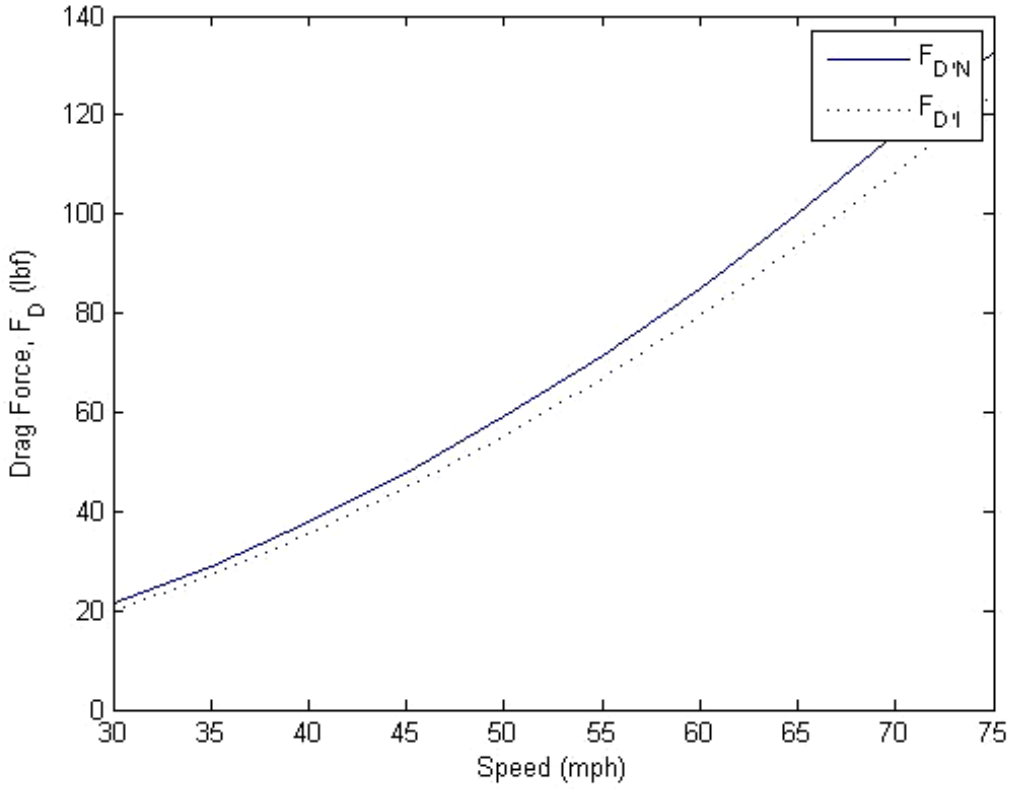

(a) Comparison of drag forces with aerodynamically improved designs at varying vehicle speeds

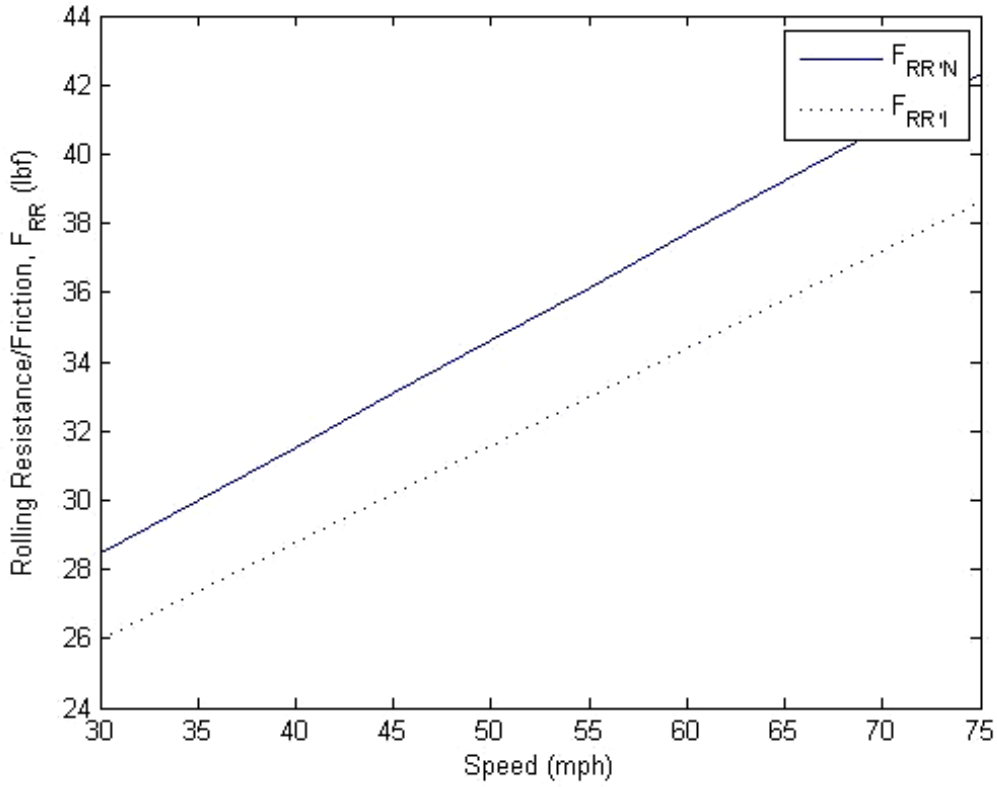

(b) Comparison of frictional forces with lighter body weight at varying vehicle speeds

Figure 10. (Continued)

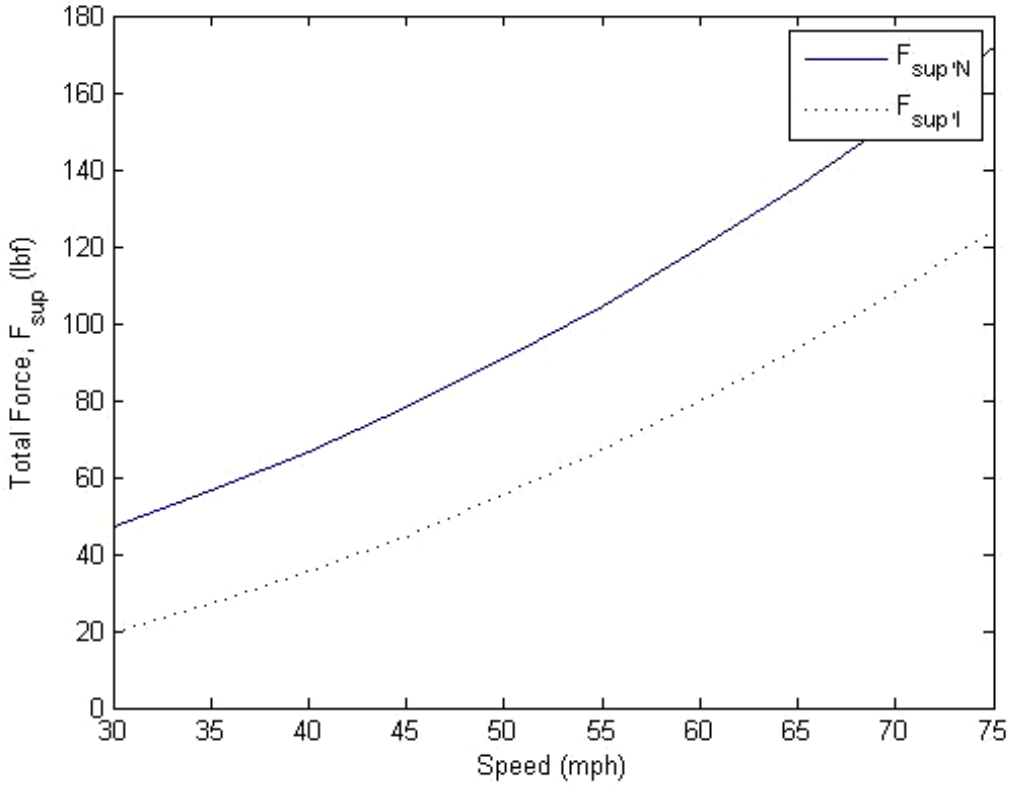

(c) Comparison of total forces with lighter aerodynamically sound designs

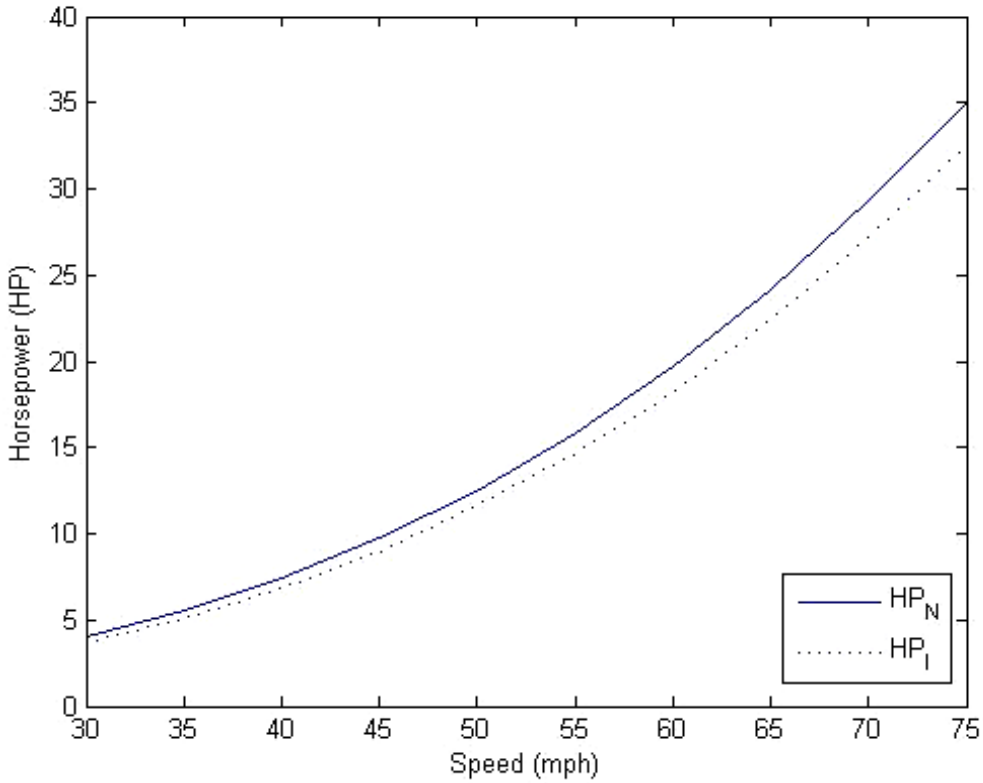

(d) Horsepower Comparisons with optimized total supplied forces

Figure 10. Optimized performance parameters

5. Conclusion

CFD analysis conducted during the design phase of an automobile allows for engineers and designers to improve designs and monitor resulting changes in the car's future performance. Other factors like cost and weight can introduce constraints to certain design changes. For instance, adding the wheel skirt as shown in the example will add weight to the overall car. This will affect the horsepower required by the car. Since, the supplied force is the sum of force lost to drag and at the wheels due to friction [16].

Using more streamlined and lightweight vehicle body panels can reduce drag and rolling resistance forces and lead to more power being available to the wheels than being used up in counteracting the fractioning forces that is opposing the motion of an automobile. Figure 10 shows the improved performance curves after a 168 lb reduction in weight by changing the material from conventional sheet metal to lighter composites, as well as a 0.028 reduction of the coefficient of drag (C_D). This resulted in a 7.24 % reduction of the required horsepower, resulting further is less consumption of fuel by the automobile engine.

Nomenclature

A	Area, Vehicle Frontal Area
CAD	Computer Aided Design
CFD	Computational Fluid Dynamics
C_D	Coefficient of Drag
D	Equivalent Length
d	Distance
E_k	Kinetic Energy
F_D	Drag Force
F_i, f	Force at inlet and outlet; external forces
FEM	Finite Element Method
g	Gravitational Constant
H	Total Energy Head
h	Hydraulic Head or Fluid Height
K	Constant (in Bernoulli)
m	Mass
p_i	Pressure
p_0	Total Pressure
q	Dynamic Pressure Head
Re	Reynolds Number
S	Strain Tensor Rate
t	Time
u	Velocity
v_0	Initial Velocity
W	Work done on, by the system
z_i	Heights

Greek Symbols

μ	Kinematic Viscosity
ρ	Density
v	Fluid Viscosity
τ	Variable to quantify the filtered and unfiltered speed variables
δ	Isotropic Stress Component
v	Apparent Stress Coefficient

Subscripts

air	Air at standard temp and pressure
frontal	Front View of the car
scale	Model Size
full	Real Life car size
g	referring to, or due to gravity
k	referring to, or due to kinetics
t	referring to, or due to totality
p	referring to, or due to pressure
max	Maximum value
min	Minimum value
x	X Component
y	Y Component
z	Z Component
i,j	Spatial Components

References

[1] Obayashi S., Fujii K., Gavali S. Navier-Stokes simulation of wind-tunnel flow using LU-ADI factorization algorithm, National Aeronautics and Space Administration (NASA), Ames Research Center, 1998.

[2] Batchelor, G. K. An Introduction to Fluid Dynamics, Cambridge University Press 1967, ISBN 0521663962.

[3] Orszag S.A. Analytical Theories of Turbulence. Journal of Fluid Mechanics 1970, 41, 363–386.

[4] Yokokawa M., Itakura K., Uno A., Ishihara T., Kaneda Y. TFlops Direct Numerical Simulation of Turbulence by a Fourier Spectral Method on the Earth Simulator, Proceedings of the ACM/IEEE Conference on Supercomputing, Baltimore MD, 2002.

[5] Buckingham, E. On physically similar systems; illustrations of the use of dimensional equations. Phys. Rev. 1914, 4, 345–376.

[6] Bernoulli, D., Bernoulli J. Hydrodynamics and Hydraulics (Phoenix Edition). Dover Publications 2004, ISBN 978-0486441856
[7] Tipler, P. Physics for Scientists and Engineers: Mechanics (3rd Extended Edition). W. H. Freeman 1991, ISBN 0-87901-432-6., pp. 138.
[8] Feynman, R.P.; Leighton R.B.; Sands M. The Feynman Lectures on Physics 1963. ISBN 0-201-02116-1., Vol. 1, §14–3, pp. 14–4
[9] Oertel H.; Prandtl L.; B?hle, M.; Mayes K. Prandtl's Essentials of Fluid Mechanics. Springer 2004, pp. 70–71, ISBN 978-0760306963.
[10] Pitsch Heinz "Large-Eddy Simulation of Turbulent Combustion". Annual Review of Fluid Mechanics 2006, 38, 453–482.
[11] Wagner, Claus, Hüttl, Thomas and Sagaut, Pierre. Large-Eddy Simulation for Acoustics. Cambridge University Press 2007. ISBN 9780521871440.
[12] Stoll, Rob; Porté-Agel, Fernando "Large-Eddy Simulation of the Stable Atmospheric Boundary Layer using Dynamic Models with Different Averaging Schemes". Boundary-Layer Meterology, 2008, 126: 1–28. doi:10.1007/s10546-007-9207-4.
[13] Elman. "A taxonomy and comparison of parallel block multi-level preconditioners for the incompressible Navier–Stokes equations". Journal of Computational Physics 2008, 227 (3). doi:10.1016/j.jcp.2007.09.026.
[14] Sunny, S.A. Study of the Wind Tunnel Effect on the Drag Coefficient (CD) of a Scaled Static Vehicle Model Compared to a Full Scale Computational Fluid Dynamic Model. Asian J of Sci Res. 2011, 4(3) 236 –245. doi: 10.3923/ajsr.2011.236.245.
[15] Aird F. Automotive Math Handbook, Motorbooks; 1st Edition 2000, ISBN 978-0760306963 .
[16] Ehsani M., Gao Y., Gay S.E., Emadi A. Modern Electric, Hybrid Electric, and Fuel Cell Vehicles: Fundamentals, Theory, and Design, CRC Press 2009, 2nd Edition ISBN 978-1420053982

Sanwar A. Sunny is a Mechanical Engineer, who graduated from the School of Engineering at the University of Kansas, in Lawrence KS, USA. He is a former US Department of State Kennedy-Lugar Fellow/Scholar (2005-2006), and a recipient of the Robert M Carey Merit Scholarship (2006-2007) at the Kansas School of Engineering. A founding member of the Sustainable Automotive Energy Infrastructure (KU Ecohawks) Project in 2008, his research funded by the Kansas Transportation Research Institute explored the relationship between dynamic external frictional forces and automotive fuel efficiency. In 2009, he was on a team that converted a non functional gasoline automobile into a series hybrid that ran on battery packs and biodiesel made from used cooking oil (waste); KU Libraries use such converted vehicles to deliver campus mail and for other miscellaneous activities. The same year he was a distinguished merit award recipient of the KU International Programs: Global Awareness Program (GAP) and was a former ambassador for it, the previous year (2008), he also received an award from KU Service Learning Center (CSL) the same year. In 2010, he worked as an Associate Project Manager for the United States Department of Energy (USDOE) Biofuels Project in Labelle, FL. He is an initiated Member of the Pi Kappa Alpha Fraternity, the American Society of Mechanical Engineers (ASME) and the Society of Automotive Engineers (SAE). His interests include Renewable Energy Technologies (RETs), Smart Grid, Green Buildings, WtE Processes, Automotive Design and Energy policy.
E-mail address: sanwar@ku.edu

